15th World Congress on Computational Mechanics (WCCM-XV)
8th Asian Pacific Congress on Computational Mechanics (APCOM-VIII)
Virtual Congress: 31 July – 5 August 2022
S. Koshizuka (Ed.)

THE EFFECT OF PARTICLE SHAPE ON ROCKFALL EVENTS

RYOTA SHIYAKE[1], DOMINIK KRENGEL[2] AND MAMORU KIKUMOTO[3]

[1] Yokohama National University
Tokiwadai 79-5, Hodogaya, Yokohama, Kanagawa 240-8501,Japan,
shiyake-ryota-bp@ynu.jp

[2] University of Tsukuba
1-1-1, Tennodai, Tsukuba, 305-8573, Japan
Krengel.dominik.kb@u.tsukuba.ac.jp

[3] Yokohama National University
Tokiwadai 79-5, Hodogaya, Yokohama, Kanagawa 240-8501,Japan
kikumoto-mamoru-fc@ynu.ac.jp

Keywords Granular materials, DEM, Shape, Rockfall, Trajectory

Abstract. The effects of rock shape and initial orientation on the rockfall phenomena are studied using a two-dimensional polygonal discrete element method (DEM). In the simulation, rock particles with the same mass but different shapes are dropped from the same height onto a straight slope to investigate the variations in both translational and rotational kinetic energies and the runout distance. Parametric studies under varied angularity and aspect ratio of the rock revealed a significant effect of rock shape and initial orientation on the runout distance.

1 INTRODUCTION

Rockfall is a significant and frequently occurring geohazard in mountainous areas and on engineered slopes. A (usually angular) mass of rock detaches from a bedrock slope and rapidly moves down-slope, involving freefall, bouncing, rolling, and sliding, which significantly alters the rock's behavior [1, 2, 3]. The high kinetic energy of the rock and the unpredictability of its trajectory and frequency of occurrence means that rockfall poses a major risk to human life and infrastructure, e.g. [4]. While rockfall is, in principle, fully described by a rigid body motion, the shape and orientation of the rock, constitution of the terrain, and interaction between the rock and the terrain significantly complicate the issue. Therefore, countermeasures not only include predicting the occurrence of rockfall events [5], but also estimating their runout paths and dynamics [2, 6, 7, 8] to design appropriate mitigation structures. Field tests and experiments are reasonable ways to evaluate the risk posed by rockfalls. Still, they are difficult to perform, require lots of manpower and time, and are consequently very limited in scope.

On the other hand, numerical simulations are not subject to such restrictions. In particular, the discrete element method (DEM) is ideally suited to model rockfall issues, as the rock can be modeled as a single rigid particle of arbitrary shape. Following classical point-mass models, the simplest approaches assume the rock to be a homogenous disc in two-dimensional geometries, rolling down a simple slope [9]. While these models are easy to implement, the behavior of round and non-round particles are fundamentally different, and thus their predictive power is low. More sophisticated DEM models can represent arbitrarily shaped rocks as an agglomerate of interconnected discs or spheres. The connection between individual particles in the cluster can be rigid or elastic, allowing deformation of the rock to some extent. The most recent DEM rockfall simulations use polyhedral particles of arbitrary convex shape in three-dimensional environments and often implement complex contact laws to account for impact mechanics and rock scarring.

This paper aims to study the effects of shape and initial orientation of rock on rockfall behavior through a two-dimensional polygonal discrete element method. Parametric studies of rockfall events for various rocks of different angularities and aspect ratios are carried out. The effects of shape on the runout behavior of rocks and the related mechanism are discussed based on translational kinetic energy and angular kinetic energy.

2 Simulation

2.1 Polygonal DEM

We employ a two-dimensional polygonal discrete element method based on [10] to model the rockfall behavior of elongated and non-elongated angular particles. The physical deformation of the particle upon contact is modeled as an overlap of the particle with the ground. The connecting line between the intersection points S_1 and S_2 defines the tangential direction (t). Consequently, the normal direction (n) is also fixed. An example of the interaction geometry is given in Figure 1, left. The interaction forces apply to the centroid (P) of the overlap area. The elastic normal force is a function of the overlap area A, i.e., the particle deformation and Young's modulus Y as

$$\boldsymbol{F}_{el} = Y\frac{A}{l} \tag{1}$$

with the characteristic length

$$l = 4\frac{\mathbf{r}_1\mathbf{r}_2}{\mathbf{r}_1 + \mathbf{r}_2} \tag{2}$$

for the contact vectors $\mathbf{r}_1$ and $\mathbf{r}_2$. Normal dissipation is modeled with respect to the deformation rate $\dot{A}$ as

$$\boldsymbol{F}_{diss} = \gamma\sqrt{mY}\frac{\dot{A}}{l} \tag{3}$$

with the reduced mass m of the contacting particles and damping constant γ. An additional cutoff is required to prevent the dissipative force from overcompensating the elastic force. The normal force $\boldsymbol{F}_{\mathrm{N}}$ then is the sum of the elastic normal force and the dissipative normal force. Solid friction is implemented in a tangential direction with a Cundall-Strack [11] formulation

$$\boldsymbol{F}_{\tan}(t) = \begin{cases} \boldsymbol{F}_{\tan}(t-\delta t) - k_{\tan}\Delta t v_{\mathbf{tan}}, & |\boldsymbol{F}_{\tan}(t)| \le \mu\boldsymbol{F}_{\mathbf{N}} \\ \mathrm{sgn}\big(\boldsymbol{F}_{\tan}(t-\Delta t)\big)\mu\boldsymbol{F}_{\mathrm{N}}, & |\boldsymbol{F}_{\tan}(t)| > \mu\boldsymbol{F}_{\mathbf{N}} \end{cases} \tag{4}$$

where $v_{\tan}$ is the tangential velocity and $k_{\tan}$ is the tangential stiffness of a spring, and Δt the timestep of the simulation. The torques are computed from the sum of the normal and tangential forces F and the contact vectors $\mathbf{r}_1$ and $\mathbf{r}_2$ as

$$\boldsymbol{T}_{\mathbf{1,2}} = \mathbf{r}_{\mathbf{1,2}} \times \mathbf{F}\,. \tag{5}$$

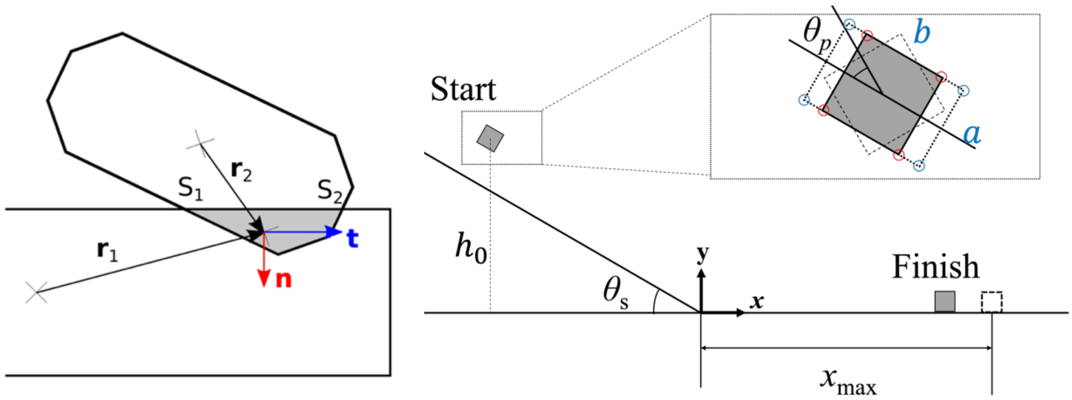

Figure 1 *Left* : Contact geometry for polygonal particles. The vectors $\mathbf{r_1}$ and $\mathbf{r_2}$ connect the particle center-of masses and the centroid P of the overlap area (dark shading). The normal (*n*) and tangential (*t*) direction of the contact are given by the intersection points S_1 and S_2 of the overlap.
Right : Visualization for the initial geometry. A particle with axes *a* and *b* is placed above a slope at a height h_0 and an initial orientation θ_p.

Table 1 Particle shape and elongations considered in the simulation

	N = 4	N = 8	N = 16
	Case 1	Case 3	Case 5
a/b = 1.0	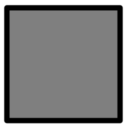	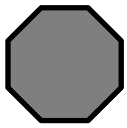	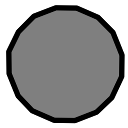
	Case 2	Case 4	Case 6
a/b = 1.4		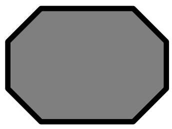	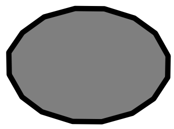

Table 2 Material parameter.

Initial height	h_0	0.3 [m]	Friction coefficient	μ	0.445
Slope angle	θ_s	30 [°]	Young's modulus	Y	10^9 [N/m]
Mass	m	262.5 [g]	Timestep	Δt	1.0×10^{-6} [1/s]

2.2 Simulation patterns

Figure 1 right shows an example of the simulation setup. The ground is modeled as a straight slope with an inclination angle of θ_s = 30° and a horizontal plane below the slope. For each simulation, the particle is placed with its center at equal heights h_0 above the slope to maintain the same initial conditions. The particles are convex polygons with 4, 8, and 16 corners with equal semi-axes a, b, and with an aspect ratio of $b/a = 1.4$, see Table.1 for an overview. For all particles, we perform 90 simulations with different initial orientations θ_p. The range of θ_p is limited by the symmetry of the particle: For all elongated particles, $\theta_p$varies in $[-90° + 90°$ with respect to the long side being parallel to the slope. For *N* = 4θ_p is limited to $\pm 45°$, for *N* = 8 to $\pm 22.5°$, and for *N* = 16 to $\pm 11.25°$. To make the simulations more comparable, all particles have the same mass regardless of their shape. The parameters are given in Table 2.

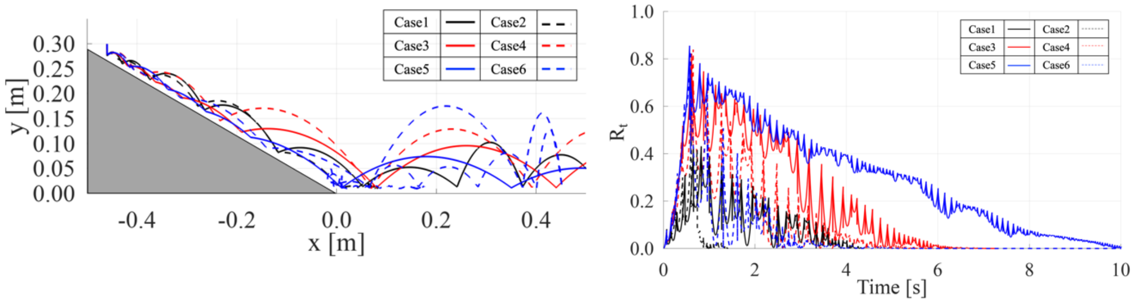

Figure 2 *Left*: Trajectories of differently shaped particles with the same initial orientation.
Right: Evolution of the relative total energy for different particles with the same initial orientation

Upon simulation start, the particle is dropped under gravity onto the slope, from where it moves until it comes to rest on the horizontal plane. However, the final position of the particle may differ from its maximum runout distance x_{max}, as the particle may bounce backward. In this research, any mention of runout distance refers to the maximum runout distance.

2.3 Energy-based discussion of the rockfall mechanism

In this paper, the behavior of the falling rock particle is discussed based on energy. The total energy of the rock particle is given by the summation of the gravitational potential energy E_g, the kinetic energy E_k.

$$E_t = E_g + E_k \tag{6}$$

The gravitational potential energy is given as

$$E_g = mgy_g \tag{7}$$

where m is the mass of the particle and y_g is the vertical coordinate of the particle's center of gravity. The kinetic energy of the particle is given by the sum of the translational kinetic energy, E_{kt}, and the angular kinetic energy, E_{kr}.

$$E_k = E_{kt} + E_{kr} = \frac{1}{2}m\mathbf{v}^2 + \frac{1}{2}I\omega^2 \tag{8}$$

Here, v is the velocity vector, I is the moment of inertia, and ω is the angular velocity.

Initially, the rock particle is at rest in the air, so both kinetic and elastic energy are zero.

$$E_{k0} = E_{e0} = 0 \tag{9}$$

Therefore, the initial total energy is

$$E_{t0} = E_{g0} = mgy_{g0} \tag{10}$$

where y_{g0} is the initial height of the center of the gravity. The relative total energy is finally given as equation (11).

$$R_t = \frac{E_t}{E_{t0}} \tag{11}$$

3 Results and discussions

When we vary the particle shape, we obtain significantly different trajectories for the particles, even with the same initial orientations, see Fig. 2 (left). While the terrain is smooth in all cases,

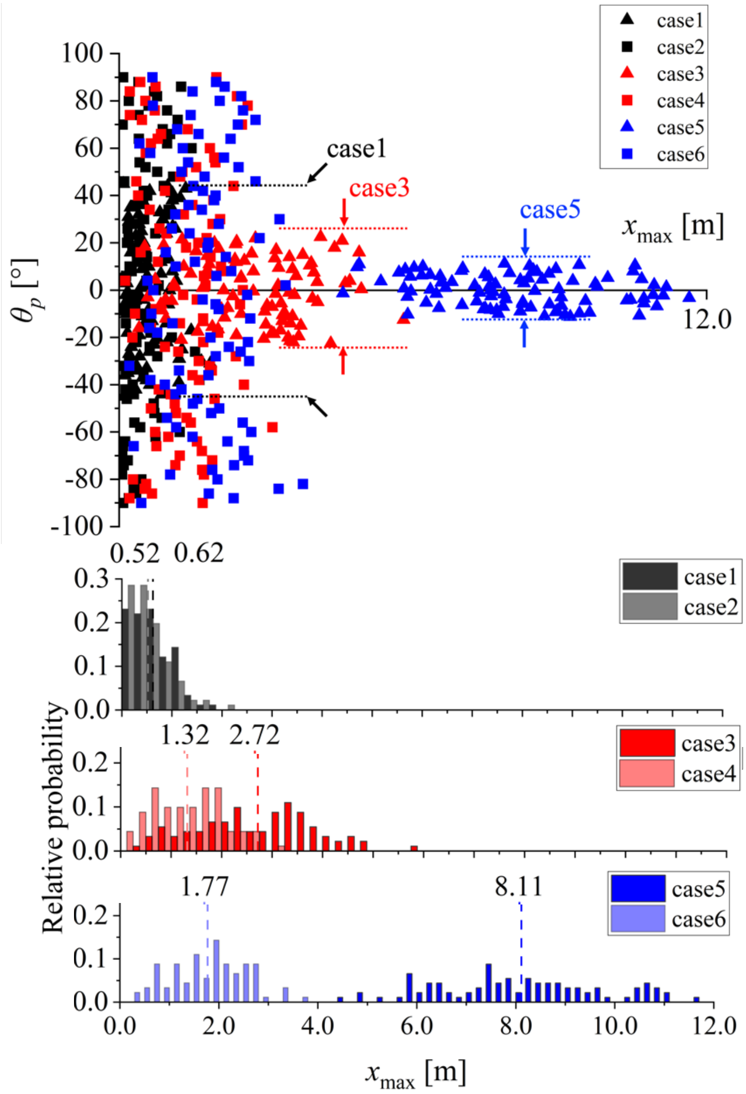

Figure 3 *Top:* Distribution of the maximum runout distances for all case with respect to the initial orientation of the particle. Due to symmetry of the particle shape, the range of θ_p is different for each non-elongated case. *Bottom*: Relative probabilities of the runout distribution with respect to the particle initial orientation and the mean runout distances for particles with 4 corners (top), 8 corners (center), and 16 corners (bottom).

differences in shape lead to difference in interaction force magnitudes and torques, in particular if the particle is elongated, and thus to differences in modes of transportation, i.e. bouncing, rolling or sliding. Figure 2 (right) shows the time evolution of the relative total energy for particles with different shapes, but the same initial orientation. As the particles are dropped from an initial distance to the slope, the primary mode of transportation that develops is bouncing, expressed by sudden spiking of the energy, where part of the kinetic energy is temporarily stored as elastic energy. This limits the energy loss by friction and increasing the total runout distances for all particles.

Like with shape, for the same particle, differences in the initial orientation can result in significant differences in the maximum runout distance as shown in Figure 3 (top), and a small

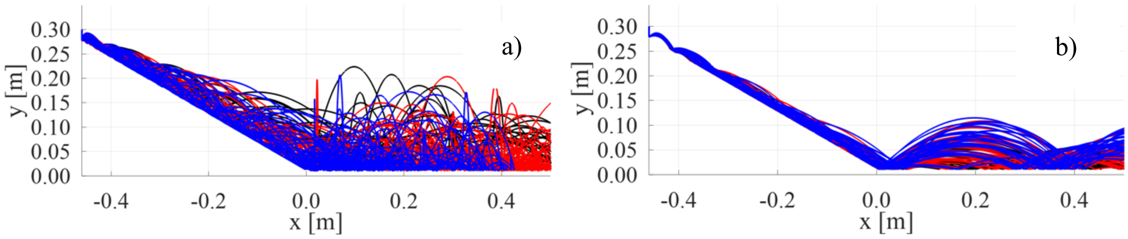

Figure 4 a) Trajectory family for N=04, a/b = 1.0. **b**) Trajectory family for N=16, a/b = 1.0. Coloring according to different runout distances: Red = long, black = median, blue = short.

change of even a few degrees may lead to large changes in the runout distance. On the other hand, the more round and spherical a particle becomes, the less its runout depends on the initial orientation, as the interaction with the floor becomes more isotropic. However, we also find that while elongation does decrease the mean runout distance, it also seems to decrease the scattering of the maximum runout. This becomes particular obvious for our case 5, a regular polygon with 16 corners, where the scattering in the runout distance is actually the largest among all cases, whereas for ideal round particles, one would expect no influence of the initial orientation at all, see Fig. 3 (bottom).

The most likely explanation is, that for 16-corner particles the angle of reflection is very similar to the impact angle, thus the particle will generally retain its forward momentum. The retained forward momentum leads to larger runout distances, which gives differences in the behavior resulting from the initial orientation more time to change the particle trajectory, see Figure 4 (b), where the trajectories follow very similar paths for all initial orientations. On the other hand, for very angular or elongated particles, impact angle and angle of reflection may differ strongly, and the differences arising from different initial orientation are strong and immediate, see Figure 4 (a), where the family of trajectories appears almost chaotic, and thus runout distances are more likely to be distributed within more narrow ranges.

In the remainder of this section we discuss differences between case 1 (N=04, a/b = 1.0) and Case 5 (N=16, a/b = 1.0). Since all particles have the same mass and same initial height, their total energy equals their initial gravitational potential and is equal for all cases. Figure 5 shows the relationship between runout distance x_{max} and total kinetic energy E_k, translational kinetic energy E_{kt}, and rotational energy E_{kr} upon first contact with the horizontal plane. As the particle travels down the slope to reach the horizontal plane, part of its energy is converted into translational and rotational kinetic energy while the rest is dissipated through collisions and sliding friction.

For the more angular particle in Case 1, if the total energy is low, then the runout distance, x_{max}, tends to be shorter. On the other hand, a higher total kinetic energy does not equate higher runout distance, as even fast particles can stop close to the slope. We further note, that most of the total kinetic energy is converted into translational kinetic energy and only a small amount into rotational kinetic energy, which does not appear to affect the runout distance much.

The more round particles in Case 5 dissipate energy much slower on the way down the slope, and therefor retain more energy on the first contact with the horizontal plane, regardless of the initial orientation. Compared to Case 1, the energy distribution for Case 5 is much more narrow and located in the upper limits of Case 1. As with Case 1, most of the energy is converted into translational kinetic energy, however the proportion of the rotational kinetic energy is much

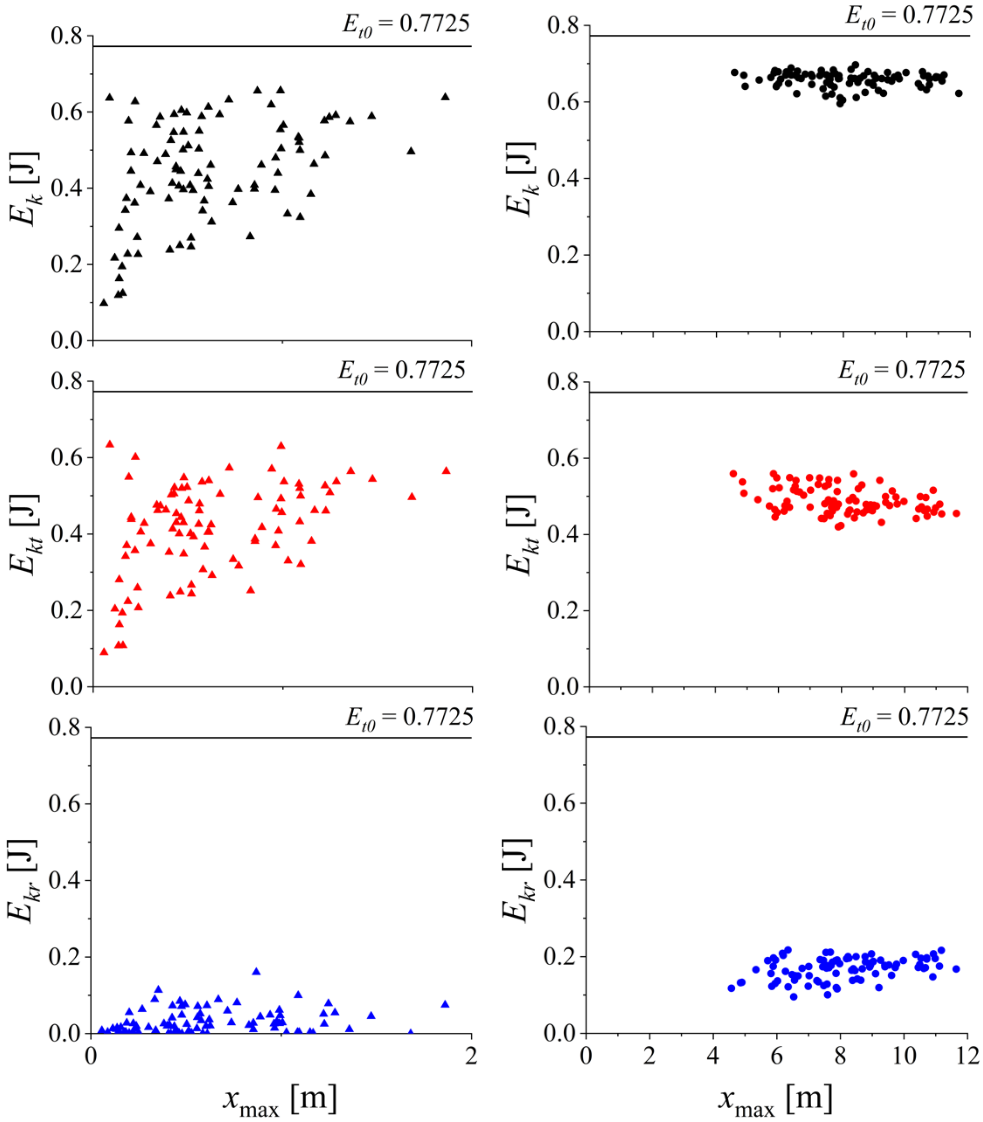

(a) Case1 (b) Case5

Figure 5 Energy upon impact on the flat ground with respect to the maximum runout distance achieved by the particle for (a) Case 1 (left column) and (b) Case 2 (right column). Note that the scale of the x-axis is different for the left and the right column.

larger for Case 5, which seems to greatly affect the runout distance. Still, the magnitude of the runout distance does not appear to be the sole determining factor of the particle runout distance.

To investigate the reason behind the significant differences in rotational kinetic energy for Cases 1 and 5, we compare the variation in angular velocity ω up to the contact with the horizontal plane, see Figure 6. here, positive angular velocity denotes clockwise rotation, negative angular velocity counter-clockwise rotation. In case of the angular particle, Case 1, the particle repeatedly gains and loses angular momentum so that its total cumulative angular velocity when reaching the horizontal plane is small. Neither for the largest, nor the shortest runout distance does the particle gain any notable rotational velocity. On the other hand, the

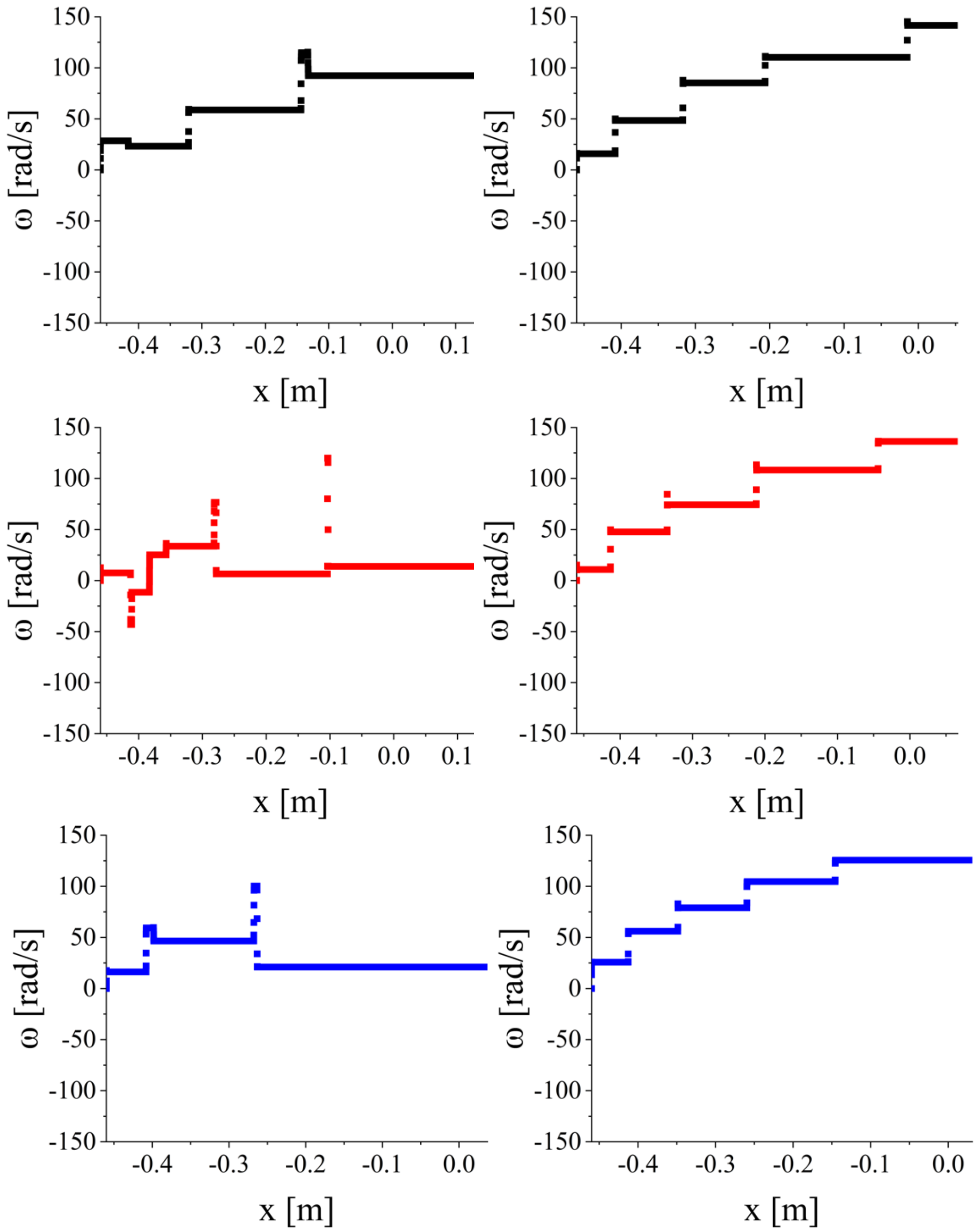

(a) Case1 (b) Case5

Figure 6 Evolution of the angular velocity ω shortly before and upon impact with the flat ground for squares (left column) and circles (right column) with the median (black), the shortest (red), and with the longest runout distance (blue).

rounded particle in Case 5 gains angular velocity in forward rotation direction with each contact with the slope. Upon reaching the horizontal plane its total angular velocity then is large, regardless of the initial orientation and eventual runout distance.

Based on the above results, it appears that the runout distance of the particles is strongly correlated with their angular velocity at contact with the horizontal plane. We summarize the

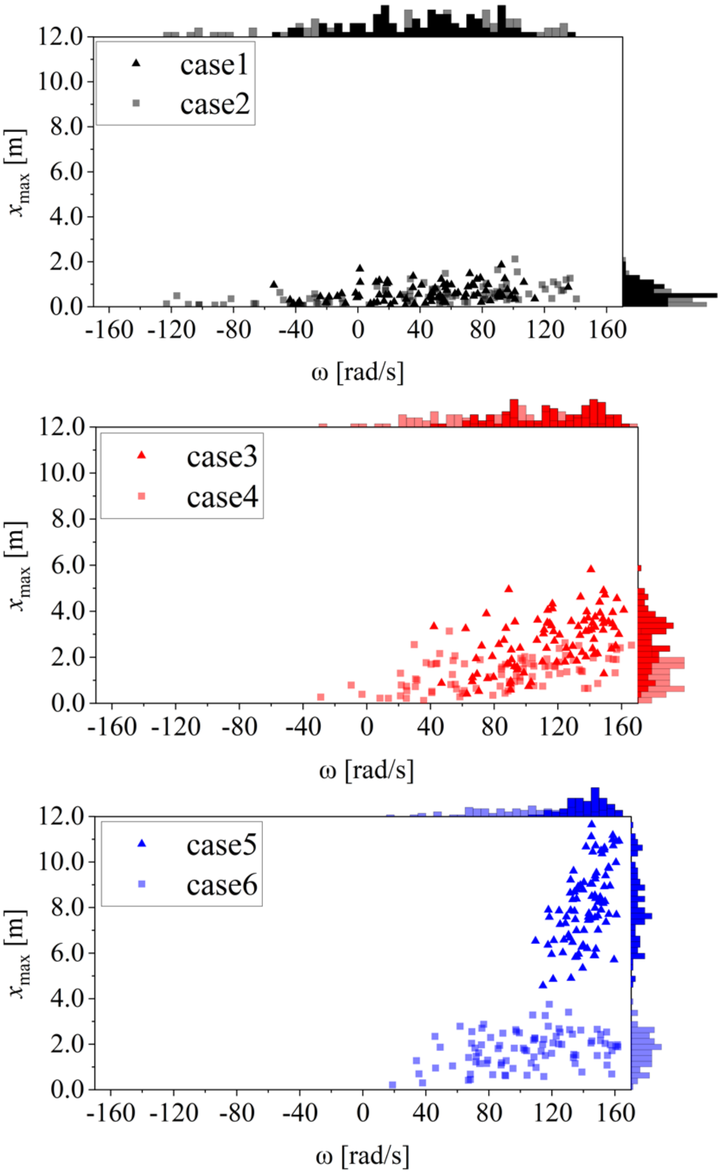

Figure 7 Correlation between angular velocity and Maximum runout distance when reaching horizontal plane (top: Case 1, Case 2), (Middle: Case 3, Case 4), (Bottom: Case 5, Case 6)

relation between angular velocity upon the first arrival on the horizontal plane and the runout distance for all cases in Figure 7. Depending on both on the particle shape and the magnitude of the angular velocity in a forward direction, the runout distance increases or decreases. We further note that for very angular particles elongation shows little influence on the correlation between angular velocity and runout distance, whereas for very round particles we observe a clear separation between elongated and non-elongated particles.

4 CONCLUSIONS

While most numerical studies of rockfall phenomena have focused on the effects of terrain topography, we investigated the effects of shape and initial orientation of the rocks on the runout distance and explored the differences in runout distance through the translational kinetic energy and the rotational kinetic energy. Through an extensive series of simulations, we derived the following conclusions:

1. There is a correlation between particle shape and initial orientation, but due to the isotropic nature of the particles, the correlation weakens as sphericity and roundness increase.
2. For very angular or elongated particles, a small change in initial orientation can cause a large change in maximum runout.
3. The maximum runout distance depends on the angular velocity upon contact with the horizontal plane.
4. The more angular particles are, the less influence the elongation has on the runout distance.

While we have used idealized convex particles, more realistic approaches using irregular, or even non-convex, particles will likely find a larger scattering of the data towards lower runout distances. Nevertheless, the gained insights on the effects of particle shape and initial orientation may be of use to create improved three-dimensional simulations.

REFERENCES

[1] De Blasio, F. V. *Introduction to the Physics of Landslides*. Springer, (2011).
[2] Ritchie, A. Evaluation of rockfall and its control. *Highway Research Record* (1963) 17: 13–28.
[3] Volkwein, A. and Schellenberg, K. and Labiouse, V. and Agliardi, F. and Berger, F. and Bourrier, F.and Dorren, L. K. A. and Gerber, W. and Jaboyedoff, M. Rockfall characterisation and structural protection – a review. *Nat. Hazards Earth Syst. Sci.* (2011) 11: 2617–2651.
[4] G. Chen et al. Numerical Simulation in Rockfall Analysis, *Rock. Mech. Rock. Eng.* (2013) 46:527—541.
[5] Frattini, P. and Crosta, G. and Carrara, A. and Agliardi, F. Assessment of rockfall susceptibility by integrating statistical and physically-based approaches. *Geomorphology* (2008) 94: 419–437.
[6] Glover, J. and Bartelt, P. and Christen, M. and Gerber, W. Rockfall-Simulation with Irregular Rock Blocks. *Engineering Geology for Society and Territory – Volume 2.* Springer, (2015).
[7] Cui, S.-h. and Pei, X.-J. and Huang, R.-Q. Rolling motion behavior of rockfall on gentle slope: an experimental approach. *J. Mt. Sci.* (2017) 14: 1550–1562.
[8] Leine, R. I. and Schweizer, A. and Christen, M. and Glover, J. and Bartelt, P. and Gerber, W. Simulation of rockfall trajectories with consideration of rock shape. *Multibody Syst. Dyn.* (2014) 32: 241–271.
[9] W. Shen et al. Discrete Element Analyses of a Realistic-shaped Rock Block Impacting Against a Soil Buffering Layer, *Rock. Mech. Rock. Eng.* (2020) 53: 3807–3822.
[10] Matuttis, H.-G. and Chen, J. Understanding the Discrete Element Method. Wiley, (2014).
[11] Cundall, P. A. and Strack, O. D. L. A discrete numerical model for granular assemblies. *Geotechnique* (1979) 29: 47–65.